Geophysical Research Letters

RESEARCH LETTER
10.1029/2025GL116960

Interplay of Submesoscale Current and Thermal Feedbacks: A Seasonal Perspective in the Gulf Stream

Lionel Renault[1], **Carlos Conejero**[1,2], **Jacob Wenegrat**[3], **and Igor Uchoa**[3]

[1]Université de Toulouse, LEGOS (CNES/CNRS/IRD/UT3), Toulouse, France, [2]ENTROPIE, IRD, University of New Caledonia, University of La Réunion, CNRS, Nouméa, New Caledonia, [3]Department of Atmospheric and Oceanic Science, University of Maryland, College Park, MD, USA

Key Points:

- Submesoscale Thermal Feedback (TFB) and Current Feedback (CFB) have a strong seasonal cycle that is mainly induced by the wind strength
- TFB can offset the CFB effect on the surface stress, especially during the summer, partially canceling out the eddy killing
- The potential energy flux is influenced by both TFB and CFB, with the greatest influence of TFB during the summer

Supporting Information:

Supporting Information may be found in the online version of this article.

Correspondence to:

L. Renault,
lionel.renault@ird.fr

Citation:

Renault, L., Conejero, C., Wenegrat, J., & Uchoa, I. (2025). Interplay of submesoscale current and thermal feedbacks: A seasonal perspective in the gulf stream. *Geophysical Research Letters*, *52*, e2025GL116960. https://doi.org/10.1029/2025GL116960

Received 15 MAY 2025
Accepted 11 OCT 2025

Author Contributions:

Conceptualization: Lionel Renault
Data curation: Lionel Renault
Formal analysis: Lionel Renault, Carlos Conejero, Jacob Wenegrat, Igor Uchoa
Funding acquisition: Lionel Renault
Investigation: Lionel Renault, Jacob Wenegrat, Igor Uchoa
Methodology: Lionel Renault, Jacob Wenegrat, Igor Uchoa
Project administration: Lionel Renault
Resources: Lionel Renault
Software: Lionel Renault, Carlos Conejero
Supervision: Lionel Renault
Validation: Lionel Renault

Abstract This study examines for the first time how submesoscale oceanic features (1–10 km) interact at a seasonal scale with the atmosphere over the Gulf Stream (GS) region using high-resolution coupled simulations. Focusing on thermal and current feedbacks (TFB and CFB), we show that their combined influence peaks in summer, enhancing surface winds while partially offsetting in surface stress. This compensation reduces the stress response, especially along the GS. Seasonal coupling variations are driven by stronger TFB in summer and modulated by background wind conditions. Energy fluxes also exhibit strong seasonality: kinetic energy transfer to the atmosphere intensifies in winter, while, over the GS, potential energy gains can dominate in summer, partly influenced by CFB. These results highlight the importance of accounting for both feedbacks—and their seasonal variability—in studies of submesoscale air-sea interactions. Future satellite missions and field campaigns will be essential to validate and extend these results.

Plain Language Summary Ocean currents and the atmosphere are tightly coupled, especially at small scales of a few kilometers, known as the submesoscale. At these scales, the ocean can influence the atmosphere in two important ways: through the thermal feedback (influence of sea surface temperature, TFB) and through the current feedback (influence of sea surface current, CFB). Using high-resolution ocean-atmosphere simulations in the Gulf Stream region, we investigated how these feedbacks vary between winter and summer. We found that TFB has a stronger influence on wind patterns in summer, while stronger ocean currents lead to more energy transfer from the ocean to the atmosphere in winter. Interestingly, the two feedbacks often act in opposite directions, partially canceling each other out for surface stress. Despite these seasonal shifts in energy exchange, the small-scale response of the ocean remains relatively stable. At the smallest scales, both feedbacks are particularly active. This work contributes to our understanding of how fine-scale air-sea interactions influence the exchange of potential and kinetic energy between the ocean and the atmosphere and the associated effects on ocean dynamics.

1. Introduction

The ocean exhibits motions over a wide range of scales, from centimeters to thousands of kilometers. Mesoscale eddies, with horizontal scales of a few hundred kilometers, are among the most energetic flows, influencing marine ecosystems (e.g., Mahadevan, 2016), the carbon pump (Harrison et al., 2018), and boundary current dynamics (Chassignet & Marshall, 2008; Renault et al., 2019). Submesoscale currents, with horizontal scales of meters to tens of kilometers, are characterized by large Rossby numbers and intense vertical velocities (Capet, Mcwilliams, et al., 2008; Su et al., 2020). They influence buoyancy, momentum, and biogeochemical exchange (Kessouri et al., 2020; Lévy et al., 2009; Su et al., 2018; Wenegrat et al., 2020) and play a role in the oceanic energy cascade (Boccaletti et al., 2007; Capet, McWilliams, et al., 2008; Contreras et al., 2023a; Dong et al., 2024).

Ocean-atmosphere interactions at the mesoscale have been studied extensively in the past decades, revealing two key processes: the Thermal FeedBack (TFB) and the Current FeedBack (CFB). TFB modifies turbulent heat fluxes and affects wind speeds (see Small et al., 2008; Seo et al., 2023 for a review), while CFB directly influences surface stress, creating an ocean-to-atmosphere bottom-up effect on winds (Renault, Molemaker, McWilliams, et al., 2016). These interactions modulate ocean dynamics, with TFB reducing oceanic potential energy (Bishop et al., 2020; Ma et al., 2016; Renault et al., 2023) and CFB acting as an "eddy killer", extracting kinetic energy from eddies to the atmosphere (Renault et al., 2018; Renault, Molemaker, Gula, et al., 2016; Renault, Molemaker, McWilliams, et al., 2016).

Visualization: Lionel Renault, Carlos Conejero
Writing – original draft: Lionel Renault
Writing – review & editing: Lionel Renault, Carlos Conejero, Jacob Wenegrat, Igor Uchoa

Submesoscale air-sea interactions are not fully understood (Nuijens et al., 2024). According to Conejero et al. (2024) and Renault et al. (2024), the eddy-killing effect is more pronounced at the submesoscale than at the mesoscale due to a weaker wind response to CFB. However, the net effect of CFB is a reduction in submesoscale activity of less than 10%, compared to a 30% reduction at the mesoscale. As shown by Uchoa et al. (2025) and Renault et al. (2024), submesoscale TFB creates a potential energy sink that weakens submesoscale currents by at least 10% at scales shorter than 10 km. Recent studies by Bai et al. (2023); Conejero et al. (2024); Renault et al. (2024) show that submesoscale TFB and CFB can either enhance or counteract each other by influencing surface stress and wind anomalies, thereby affecting the exchange of kinetic energy.

Building on these findings, this study goes a step further than Renault et al. (2024), Conejero et al. (2024), and Uchoa et al. (2025) by presenting the first analysis of the seasonal cycle of submesoscale air–sea interactions in the Gulf Stream. The analysis emphasizes the spatial variability of these interactions and the role of current feedback (CFB) and thermal feedback (TFB) in shaping energy exchanges and the oceanic submesoscale kinetic energy response. Section 2 describes the numerical experiments. Section 3 traces the chain of events driven by CFB and TFB from submesoscale coupling coefficients to resulting kinetic and potential energy fluxes and, ultimately, the submesoscale kinetic energy response. Section 4 summarizes the conclusions and discusses the broader implications.

2. Methods

2.1. Numerical Experiments

We use the Coastal and Regional Ocean Community model (CROCO, Debreu et al., 2012) and the Weather Research Forecast model (WRF v.4.2; Skamarock et al., 2008), coupled via the OASIS3-MCT coupler (Craig et al., 2017). CROCO is a hydrostatic (with non-hydrostatic option), terrain-following, free-surface ocean model that adheres to the Boussinesq approximation and employs a split-explicit time-stepping scheme. Its high accuracy is achieved through a third-order predictor-corrector algorithm and advanced numerical methods, including a fifth-order upstream scheme for momentum advection and pressure gradient discretization. For tracer advection, a third-order upstream-biased scheme is used in a split configuration, with the diffusive component rotated along isopycnal surfaces to reduce unwanted diapycnal mixing (Lemarié et al., 2012; Marchesiello et al., 2009). Turbulent mixing processes that are not resolved explicitly—at the surface, bottom, and ocean interior—are represented using the K-Profile Parameterization (KPP, Large et al., 1994).

We use the same oceanic and atmospheric configurations as Renault et al. (2024). The models are implemented over the GS region and its zonal extent, as shown in Figure 1. The domain spans from 78.6°W to 55.27°W and 34°N to 42.9°N, discretized with a nominal horizontal grid spacing of approximately 700 m for the ocean and 2 km for the atmosphere. Note that the atmospheric domain is slightly more extended (by 8 km) than the ocean domain to avoid coupling with the WRF sponge. In the vertical, CROCO uses 80 sigma-levels with stretching parameters of $\theta_s = 7$, $\theta_b = 2$, and $h_{cline} = 200$ m, whereas WRF has 50 hybrid eta levels, with a model top pressure set at 1,000 Pa and a first level at 10 m over the ocean.

We performed three 12-month coupled simulations (plus 3-month of spin up, starting from April 2005), all of which account for the large-scale and mesoscale coupling between the ocean and the atmosphere:

- CTRL considers both submesoscale TFB and CFB.
- In NOTFB_SUB, the SST sent to WRF is smoothed with a 30 km Gaussian filter to remove submesoscale variability and isolate CFB effects.
- In NOCFB_SUB, the surface currents are smoothed instead, isolating TFB effects.

The exchange of coupled fields is done every hour following the procedure described in Masson et al. (2025). See Renault et al. (2024) for more details and for an evaluation of the simulations against the observations. In the following, the summer (July, August, September) and winter (January, February, March) boreal seasons are compared. Following Renault et al. (2024), submesoscale anomalies, denoted by the prime sign (’), are defined as deviations from a 2-day running mean and by applying the high-pass Gaussian spatial filter (cutoff of about 30 km) used online in NOTFB_SUB and NOCFB_SUB simulations.

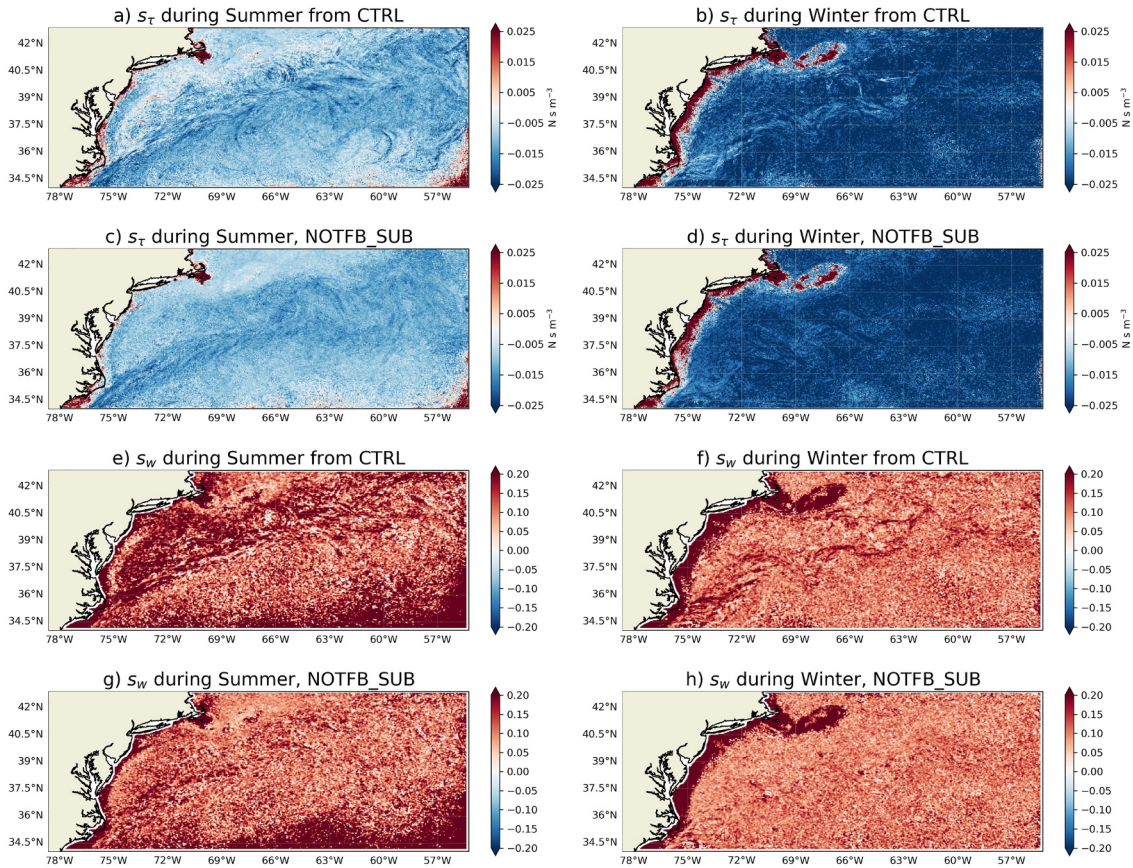

Figure 1. Coupling coefficients related to the CFB. (a, b) s_τ in summer and winter from CTRL; (c, d) s_τ in summer and winter from NOTFB_SUB (e, f, g, h) same than (a, b, c, d) but for s_w. The coupling coefficients exhibit a strong seasonal cycle that is influenced by TFB and by the wind background strength.

3. Results

3.1. Submesoscale Coupling Coefficients

Figure 1 shows two submesoscale coupling coefficients that influence the kinetic and potential energy exchanges between the ocean and the atmosphere: s_τ (Figures 1a–1d) denotes the coupling coefficient between submesoscale surface current vorticity and the curl of submesoscale surface stress. It does not directly represent the sink of kinetic energy from the ocean to the atmosphere, but instead characterizes the efficiency of "eddy killing": more negative values of s_τ correspond to a more efficient damping of submesoscale eddies. This coefficient is derived as the slope of the linear relationship between surface current vorticity and surface stress curl submesoscale anomalies.

s_w is the coupling coefficient between submesoscale surface currents vorticity and 10-m wind curl. It is estimated as the slope between surface current vorticity and 10-m wind curl submesoscale anomalies. A larger s_w indicates stronger wind curl anomalies that are positively correlated with the surface current vorticity, which weakens s_τ, that is, the CFB effects on surface stress and the eddy killing. These coefficients are estimated for both the summer and winter seasons at each grid point.

In the CTRL simulation, s_τ is characterized by a clear seasonal cycle, with more negative values in winter than in summer, indicating a more efficient eddy killing (Figures 1a and 1b). In addition, the spatial variability differs between seasons. In summer, s_τ shows strong spatial heterogeneity, with near-zero values in the northern GS region and more negative values along the GS path. In winter, s_τ is more spatially homogeneous, with values around -3×10^{-2} N s m^{-3}, except along the GS path, where values reach about -2×10^{-2} N s m^{-3}. This suggests that during winter, the eddy killing is less effective along the GS path.

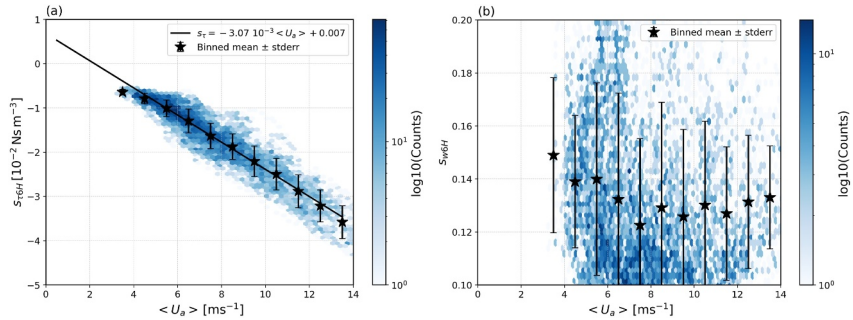

Figure 2. Binned scatterplot of the 6-hr time series of 10 m-wind magnitude domain average and (a) s_τ, (b) s_w over the full domain. s_τ and s_w are estimated each 6 hr as the slope of the linear regression between submesoscale currents anomalies and stress and wind anomalies, respectively. The colors indicate the density of the points, and the bars show plus and minus one standard deviation about the mean marked by stars. In (a), the linear regression is indicated by a black line.

The seasonal and spatial variations in s_τ can be attributed to two main factors: the submesoscale TFB effect on low-level wind and surface stress, and wind strength. As shown in Bai et al. (2023), Conejero et al. (2024), Renault et al. (2024), submesoscale TFB and CFB can have a constructive or destructive effect on surface stress and wind anomalies.

Figures 1c and 1d show s_τ from the NOTFB_SUB simulation where the submesoscale TFB is removed. In summer, compared to CTRL, the spatial heterogeneity of s_τ is reduced, especially in the northern GS region, where s_τ no longer approaches zero. Its standard deviation estimated over the domain is reduced in NOTFB_SUB with respect to CTRL from 4.4 10^{-2} versus 4.7 10^{-2} N s m^{-3} in summer. s_τ is therefore generally more negative in NOTFB_SUB, with a mean value of $-9.9\ 10^{-3}$ compared with $-9.4\ 10^{-3}$ N s m^{-3} in the CTRL run, indicating more effective eddy killing. n winter, the GS imprint on s_τ disappears in NOTFB_SUB, further reducing its spatial heterogeneity, as confirmed by a lower standard deviation across the domain. This standard deviation is reduced in NOTFB_SUB compared to CTRL in both summer and winter (4.4×10^{-2} vs. 4.7×10^{-2} N·s·m^{-3} in summer, and 1.27×10^{-2} vs. 1.30×10^{-2} N·s·m^{-3} in winter). The spatial mean of s_τ is again more negative in NOTFB_SUB than CTRL ($-18.2\ 10^{-3}$ vs. $17.5\ 10^{-3}$ N s m^{-3}). This reveals that TFB is more active in summer and along the GS path in winter, acting in a destructive way against CFB, that is, damping stress anomalies driven by CFB. Therefore, the general effect of TFB on $s_\tau$is to increase its heterogeneity, particularly along the GS path. This is likely related to the presence of strong SST fronts.

The remaining differences in s_τ intensity between summer and winter can thus be attributed to seasonal variations in wind speed. To assess its role in modulating s_τ, we estimate from CTRL s_τ every 6 hr over the entire oceanic domain, denoted as $s_{\tau 6H}$, over the entire 1-year simulation. The background wind speed $<U_a>$ is computed as the domain-averaged wind speed at the same 6-hr intervals. Consistent with the mesoscale results of Renault et al. (2017), the wind speed magnitude appears to be a good predictor of the submesoscale $s_{\tau 6H}$, with a remarkably high negative temporal correlation of −0.95. This dependence is further confirmed by statistical analysis: $s_{\tau 6H}$ values are binned as a function of $<U_a>$ using 1 m s^{-1} bins over the 12-month CTRL simulation period. The results, shown in Figure 2a, reveal a clear negative linear relationship: stronger winds lead to more negative $s_{\tau 6H}$ values. This relationship is quantified as

$$s_{\tau 6H} = -3.07 \times 10^{-3} < U_a > + 0.007 \text{ N m}^{-3}\text{s} \quad (1)$$

Note that for low wind speed, the raw data deviate from the linear relationship and the linear regression is outside of the associated standard deviation. This could be due to the wind response that is stronger for low wind speed (Figure 2b). This scaling is consistent with the mesoscale behavior reported in Renault et al. (2017, 2020), although the larger coefficients here confirm that s_τ is more negative at the submesoscale, indicating the surface stress response to CFB is stronger at these scales. Finally, this diagnostic can also be done using NOTFB_SUB and NOCFB_SUB (see Figure S1 in Supporting Information S1). From CTRL to NOTFB, the relationship between $s_{\tau 6H}$ and $<U_a>$ does not change significantly, indicating a weak influence of submesoscale TFB on this diagnostic. This

is further confirmed using NOCFB_SUB. In this case, the relationship shows a slight positive correlation, consistent with submesoscale TFB counteracting CFB: $s_{\tau 6H} = -0.1 \times 10^{-3} < U_a > + 0.0003\text{N m}^{-3}$ s.

We now assess the wind response to CFB by analyzing the s_w coupling coefficient. In CTRL, during summer, s_w is characterized by a large spatial heterogeneity, with values up to ≈ 0.25 in the northern GS region, coinciding with weaker s_τ. In winter, s_w is also characterized by the imprint of the GS path. Figures 1g and 1h shows s_w from NOTFB_SUB. As expected, in summer s_w becomes more uniform, with the high values north of the GS disappearing. In winter, the GS imprint on s_w is no longer visible. This confirms the influence of TFB on s_w and thus that TFB and CFB act together on wind and surface stress—reinforcing each other on wind and counteracting each other on surface stress. The TFB influence on s_w is stronger in summer than in winter, which is consistent with a stronger wind response to TFB in summer due to more stable atmospheric conditions and weaker wind (Desbiolles et al., 2023).

The remaining temporal variation of s_w in NOTFB_SUB is driven by wind intensity: in winter the wind is stronger, decreasing s_w and thus increasing s_τ. This is confirmed by calculating s_w every 6 hr over the entire oceanic domain, denoted s_{w6H}, over the entire 1-year simulation. The s_{w6H} values are then binned as a function of $<U_a>$ using 1 m s^{-1} bins over the 12-month CTRL simulation period. Figure 2b shows the results. Unlike $s_{\tau 6H}$, s_w shows a non-linear relationship. Two behaviors can be highlighted. For winds between 3 and 7 m $^{-1}$ (mainly occurring in summer), s_{w6H} has a linear relationship with the background wind speed $<U_a>$: the weaker the background wind speed, the stronger the response to submesoscale currents; for winds greater than 7 m s^{-1}, the s_w response reaches a plateau with a value of about 0.13 (nondimensional). Note that this value is weaker than at the mesoscale (0.3 on average), again confirming a weaker wind response to CFB at the submesoscale than at the mesoscale, and thus a larger surface stress response.

3.2. Submesoscale Potential Energy Flux

The submesoscale potential energy flux GP_s is driven by both heat flux and freshwater flux (Evaporation minus Evaporation). It has a direct influence on the oceanic buoyancy variability and, thus, on the baroclinic conversion of potential energy into kinetic energy (e.g., Bishop et al., 2020; Uchoa et al., 2025). Following Uchoa et al. (2025), we approximate the submesoscale surface buoyancy flux B_0 as

$$B_0' = \frac{\alpha_\theta g}{\rho_0 C_p} Q_{net}' - \beta_s g (SSS(E-P))' \tag{2}$$

where g is gravity, C_p is the specific heat of water, SSS is the sea surface salinity, Q_{net} is the net surface heat flux (positive values represent a flux into the ocean), and E and P are evaporation and precipitation, respectively. α_θ and β_s are the thermal expansion and salinity contraction coefficients, respectively.

The submesoscale flux of potential energy GP_s is estimated as

$$GP_s = \frac{1}{\rho_0} \frac{\overline{b_0' B_0'}}{N_r^2} \tag{3}$$

where b_0' is the surface submesoscale buoyancy ($b' = \frac{g\rho'}{\rho_0}$), and $N_r^2 = \frac{\partial <b_r>}{\partial z}$ is the reference squared Brunt-Väisälä frequency, where $<b_r> = \frac{g\rho_r}{\rho_0}$ is the horizontally and temporally averaged buoyancy over the domain and 1 year. A positive GP_s indicates a gain of potential energy for the ocean, while a negative GP_s indicates a loss of potential energy for the ocean. Figures 3a and 3e shows GP_s during summer and winter as estimated from CTRL. In CTRL, GP_s is also characterized by a strong seasonal cycle. During summer, there is a strong spatial heterogeneity with a background of positive values north of the GS (gain for the ocean) and negative values over the GS (sink for the ocean), a strong positive value over the GS separation near Cape Hatteras, and very fine-scale positive structures. Three contributions can be distinguished. First, the positive very fine-scale structures are due to the salt flux contribution and can be attributed to the interaction between mesoscale atmospheric eddies and submesoscale oceanic SSS anomalies. This can be verified by estimating GP_s from CTRL using only the submesoscale heat flux contribution that are mainly induced by TFB (GP_sQnet, Figure 3b). In GP_sQnet all very fine structures are no longer present. Estimating GP_s from NOTFB_SUB leads to the opposite, that is, a removal of all

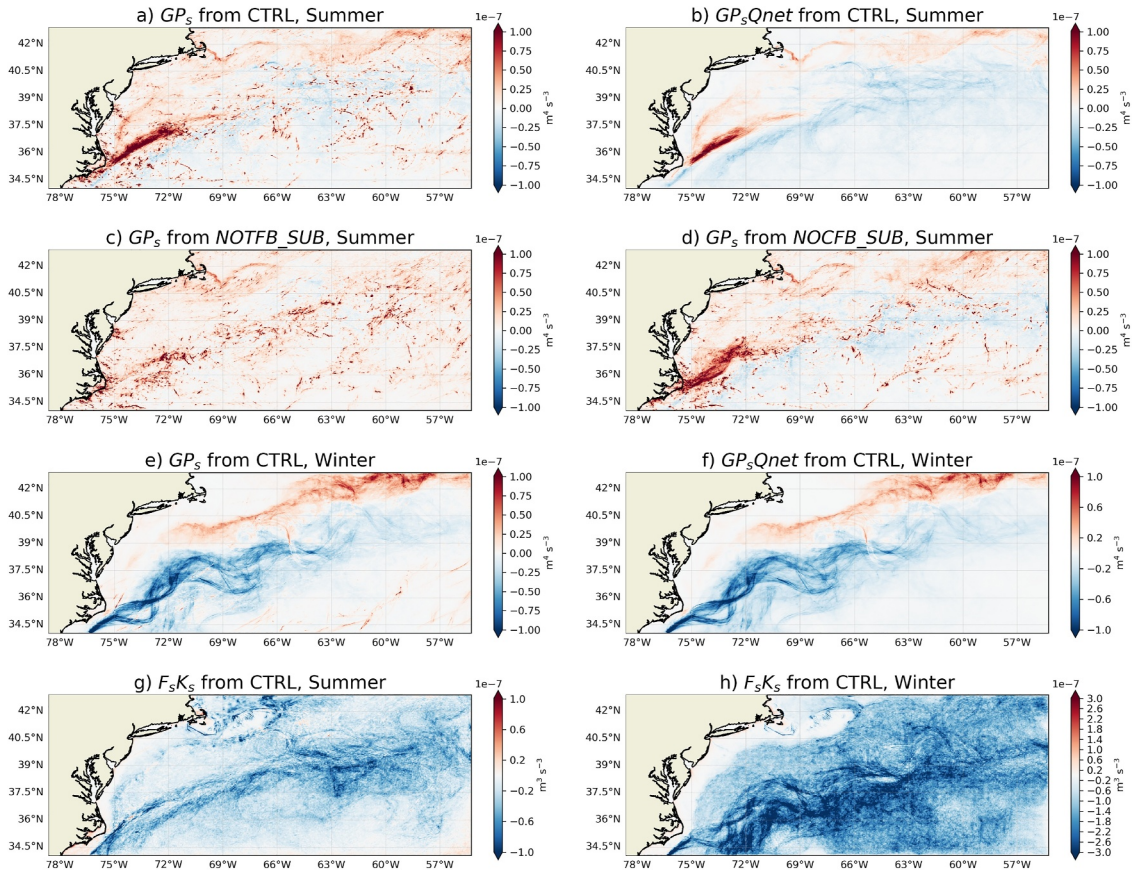

Figure 3. Submesoscale fluxes of potential (GP_s) and kinetic (F_sK_s) energy. (a, e) GP_s in summer and winter from CTRL (c, d) GP_s in summer from NOTFB_SUB and NOCFB_SUB (b, f) GP_s in summer and winter from CTRL using only the heat flux contribution (GP_sQnet). (g, h) F_sK_s in summer and winter from CTRL. F_sK_s and GP_s are characterized by a strong seasonal cycle. GP_s has contribution from TFB through SST anomalies, from CFB through the influence of surface currents on the turbulent heat fluxes, and from mesoscale convective atmospheric structures. Note the different scale range in (g, h).

but the finest structures (Figure 3c). Figure 3d shows GP_s estimated from NOCFB_SUB. In this estimate, the strong positive GP_s observed after the separation of the GS from Cape Hatteras are notably reduced (by up to 30%), highlighting the influence of CFB on GP_s. The remaining positive values result from the adjustment of SST to evaporation associated with latent heat fluxes, which enhances buoyancy anomalies (b') and thus contributes to positive GP_s values (Renault et al., 2024). The remaining negative background values reflect the transfer of heat from submesoscale oceanic structures to the atmosphere, effectively reducing the oceanic potential energy (Uchoa et al., 2025). During winter GP_s is even more dominated by the heat flux contribution (Figure 3e). Along the GS, the positive and negative values are explained by the dominance of the heat extraction (and thus potential energy removal) contribution and the salinity adjustment leading to an increase in b', the other processes being second order (e.g., the contribution of CFB represents less than 10%). GP_s can also be estimated using NOTFB_SUB, allowing to highlight the effect of CFB on GP_s. In this case, GP_s is roughly reduced by 80% with respect to CTRL, indicating an influence of CFB on GP_s by $\approx 20\%$ during winter.

3.3. Submesoscale Kinetic Flux and Energy

We now evaluate the submesoscale kinetic energy flux during summer and winter. To do this, we first estimate the submesoscale eddy windwork F_sK_s, estimated as

$$F_sK_s = \overline{\frac{1}{\rho_0}\left(\tau'_x u'_o + \tau'_y v'_o\right)} \tag{4}$$

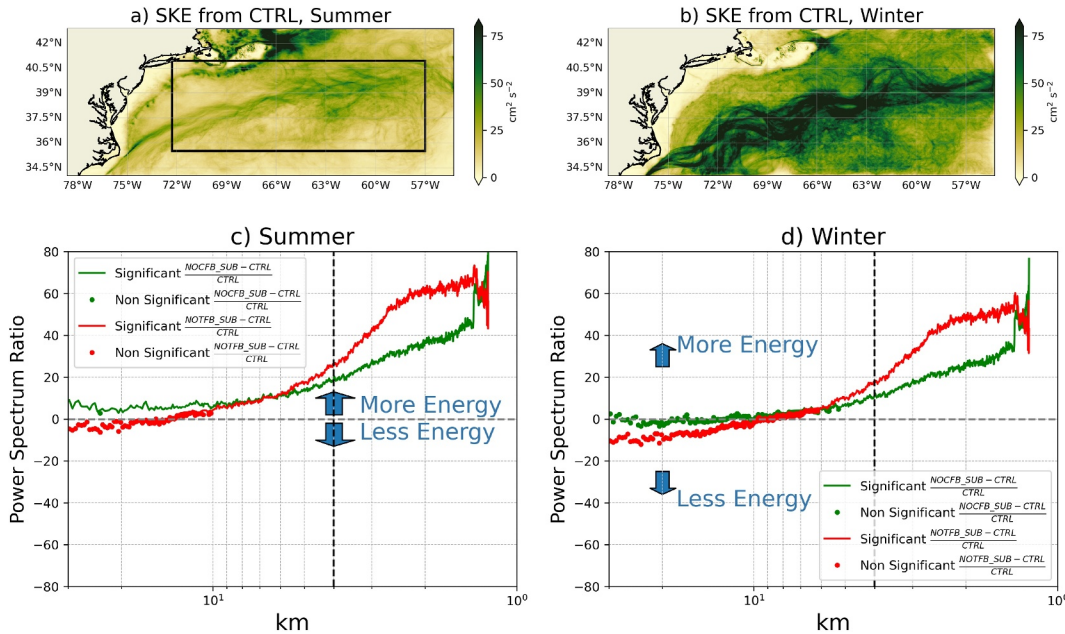

Figure 4. (a, b) Show the submesoscale kinetic from CTRL in summer and winter. (c, d) Kinetic energy co-spectrum difference between NOCFB_SUB (NOTFB_SUB) and CTRL in summer and winter. The SKE exhibits a strong seasonal cycle. Submesoscale CFB and TFB are mainly active for scales finer than 10 km. The dashed line represents approximately the effective resolution of the oceanic simulations (see Renault et al., 2024).

where τ_x and τ_y are the zonal and meridional surface stress, u_o and v_o are the zonal and meridional currents, and ρ_0 is the ocean surface density. F_sK_s represents the exchange of kinetic energy between the submesoscale currents and the atmosphere. A negative F_sK_s indicates a transfer of kinetic energy from submesoscale currents to the atmosphere.

As shown in Figures 3g and 3h, in CTRL, F_sK_s is characterized by a strong seasonal cycle with less negative values in summer than in winter and by a strong spatial heterogeneity with larger values over the GS path. F_sK_s can be approximated as the product between s_τ and the *SKE* (Renault et al., 2017) (see also Figure S2 in Supporting Information S1). s_τ has a similar seasonal cycle, with less negative values during summer than during winter, which tends to transfer less kinetic energy from the submesoscale currents to the atmosphere. Figures 4a and 4b depicts the mean Submesoscale Kinetic Energy (SKE) of CTRL for summer and winter, defined as

$$SKE = \frac{\overline{u_o'^2 + v_o'^2}}{2} \tag{5}$$

where u_o and v_o are the zonal and meridional surface currents, respectively. In agreement with the literature (e.g., Callies et al., 2015 and Contreras et al., 2023b), the SKE reaches its maximum intensity along the GS path and follows a clear seasonal cycle, with a peak during the winter months. This seasonal variation is mainly driven by mixed layer instabilities, which become more pronounced as the mixed layer deepens during winter. The seasonal variation of F_sK_s is therefore driven by both s_τ and the SKE.

3.4. Submesoscale Kinetic Energy Activity Response

To assess the submesoscale current response to CFB and TFB, the KE co-spectra are estimated according to Renault et al. (2024):

$$CS_{KE} = \overline{\int_{-100}^{0} 0.5\left(\mathbb{R}\left[\widehat{u_o}\,\widehat{u_o^*} + \widehat{v_o}\,\widehat{v_o^*}\right]\right)dz} \tag{6}$$

The caret ($\widehat{\ }$) denotes the two-dimensional Fourier transform. The symbol $\mathbb{R}$ is the real component of the spectra, and the asterisk (*) represents the complex conjugate operator.

Figures 4c and 4d shows the percentage difference between NOCFB_SUB and CTRL (green) and NOTFB_SUB and CTRL (red) for the 100 m depth-integrated KE co-spectra, averaged over the black box in Figure 4a. In contrast to the energy fluxes, both CFB- and TFB-induced SKE reductions do not show a pronounced seasonal cycle. Two scale ranges can be identified. For spatial scales in the 10–30 km range, NOCFB_SUB results in a modest reduction of the SKE (about 5%) in summer, while in winter the effect of eddy killing on the SKE is not significant in the 10–30 km range. In both seasons, the potential energy flux between the ocean and the atmosphere induced by TFB does not cause a significant modulation of the SKE. This indicates that at these scales, submesoscale TFB and CFB are not a dominant process because their relative importance is reduced compared to other processes. However, at scales finer than 10 km, both submesoscale TFB and CFB have a significant effect on the SKE, with a reduction of up to 40% for CFB and 60% for TFB. The largest reduction occurs at scales below 4 km, which corresponds to the effective resolution of the oceanic simulation that is, a gray zone where submesoscale currents are only partially (or not at all) resolved. In summer, both CFB and TFB weaken the forward cascade, with TFB additionally suppressing baroclinic energy conversion (see Figures S3 and S4 in Supporting Information S1). In winter, both feedbacks reduce baroclinic conversion, while CFB further damps the forward cascade at scales below 5 km (see Figures S3 and S4 in Supporting Information S1). Note that because of the windowing of the co-spectrum analysis, this analysis focuses on the GS vicinity, and, thus, only over the negative values of GP_s. One could expect a slight increase of the submesoscale activity nearby the GS separation during summer.

4. Conclusion and Discussion

In this study, we have investigated the seasonal variability of submesoscale CFB and TFB, including their effects on the low-level wind, surface stress, potential and kinetic energy fluxes, and the associated oceanic response. We first evaluate the coupling coefficients mainly associated with CFB: s_τ as a proxy for the surface stress response and s_w as a proxy for the wind response. Our analysis first shows that the combined effect of TFB and CFB is the strongest during summer, when they have a constructive effect on the low-level wind and a destructive effect on the surface stress. This interaction leads to a reduced CFB effect on the surface stress during summer and along the GS during both winter and summer. The seasonal evolution of the coupling coefficients can therefore be partly attributed to a stronger TFB influence during summer, as well as to the seasonal variability of the background wind speed: stronger winds lead to a weaker wind sensitivity to both TFB and CFB, resulting in a stronger surface stress response to CFB. Note that both s_τ and s_w do not fully reflect the surface stress and wind response to TFB, but only the part that is spatially coherent with the surface currents.

We then evaluated the seasonal cycle of kinetic and potential energy fluxes (F_sK_s and GP_s) induced by CFB and TFB. F_sK_s exhibits a strong modulation driven by the seasonal cycle of surface kinetic energy (SKE), with winter characterized by a larger energy reservoir, and by a more negative coupling coefficient between surface flow and stress (s_τ), which together tend to enhance the sink of kinetic energy from submesoscale flows to the atmosphere. GP_s is also characterized by a strong seasonal cycle. During summer, CFB can significantly modulate GP_s near the Gulf Stream separation and can lead to a gain of GP_s. Interestingly, while F_sK_s and GP_s are characterized by a strong seasonal cycle, the submesoscale flow response to CFB and TFB has only a weak seasonal cycle. For scales between 10 and 30 km, the SKE response is weak or even not significant, indicating that CFB and TFB are not the main drivers of their variability at these scales. In contrast, at scales below 10 km, both CFB and TFB become important.

Overall, our results highlight that CFB and TFB are inextricably linked at the submesoscale, especially in summer when submesoscale TFB can have a large influence on the low-level wind. The summer peak of TFB influence, coupled with the winter dominance of CFB-induced energy fluxes, underscores the need to consider both mechanisms simultaneously when assessing ocean-atmosphere coupling. These results also suggest that future modeling and observational efforts targeting submesoscale coupling should take into account seasonal variability, background wind conditions, and the relative strength of SST and surface current gradients. This also raises the question of how to force an ocean model at the submesoscale. We have shown that, similar to the mesoscale, the submesoscale s_τ can be predicted from the magnitude of the wind. However, the coefficients differ due to a weaker wind response at the submesoscale. In some regions during summer, TFB can also offset the effect of CFB

on surface stress. The existing CFB parameterizations proposed by Renault et al. (2020) do not account for these subtleties and should be revised to be scale-aware and to include potential combined TFB effects.

To conclude, in terms of observations, new missions such as Harmony (López-Dekker et al., 2019) and future mission such as ODYSEA (Larrañaga et al., 2025; Rodríguez et al., 2019) and intensive in situ campaigns such as the S-MODE campaign (Farrar et al., 2025) could help to have a better understanding of the seasonal cycle of the submesoscale air-sea interactions and even to derive parameterizations based on observations.

Conflict of Interest

The authors declare no conflicts of interest relevant to this study.

Data Availability Statement

The CROCO model and its toolbox are available at https://www.croco-ocean.org/. The WRF version we used can be downloaded from https://github.com/wrf-croco/.

Acknowledgments
We appreciate support from CNES TOSCA I-CASCADE, POSEIDON, and M-ODYSEA projects. This work used the GENCI (project 13051) computing resources. J.W. and I.U. gratefully acknowledge support from NASA Grants 80NSSC21K0554 and 80NSSC24K0412 awarded under NASA Research Announcement NNH20ZDA001NPO to the University of Maryland, College Park. L.R. thanks J.R.C. for fruitful discussions.

References

Bai, Y., Thompson, A. F., Villas Bôas, A. B., Klein, P., Torres, H. S., & Menemenlis, D. (2023). Sub-mesoscale wind-front interactions: The combined impact of thermal and current feedback. *Geophysical Research Letters*, *50*(18), e2023GL104807. https://doi.org/10.1029/2023gl104807

Bishop, S. P., Small, R. J., & Bryan, F. O. (2020). The global sink of available potential energy by mesoscale air-sea interaction. *Journal of Advances in Modeling Earth Systems*, *12*(10), e2020MS002118. https://doi.org/10.1029/2020ms002118

Boccaletti, G., Ferrari, R., & Fox-Kemper, B. (2007). Mixed layer instabilities and restratification. *Journal of Physical Oceanography*, *37*(9), 2228–2250. https://doi.org/10.1175/jpo3101.1

Callies, J., Ferrari, R., Klymak, J. M., & Gula, J. (2015). Seasonality in submesoscale turbulence. *Nature Communications*, *6*(1), 6862. https://doi.org/10.1038/ncomms7862

Capet, X., McWilliams, J. C., Molemaker, M. J., & Shchepetkin, A. (2008b). Mesoscale to submesoscale transition in the California current system. Part III: Energy balance and flux. *Journal of Physical Oceanography*, *38*(10), 2256–2269. https://doi.org/10.1175/2008jpo3810.1

Capet, X., Mcwilliams, J. C., Molemaker, M. J., & Shchepetkin, A. F. (2008a). Mesoscale to submesoscale transition in the California current system. Part I: Flow structure, eddy flux, and observational tests. *Journal of Physical Oceanography*, *38*(1), 29–43. https://doi.org/10.1175/2007jpo3671.1

Chassignet, E. P., & Marshall (2008). Gulf stream separation in numerical ocean models. *Ocean Modeling in an Eddying Regime*, 39–61. https://doi.org/10.1029/177gm05

Conejero, C., Renault, L., Desbiolles, F., McWilliams, J., & Giordani, H. (2024). Near-surface atmospheric response to Meso-and submesoscale current and thermal feedbacks. *Journal of Physical Oceanography*, *54*(3), 823–848. https://doi.org/10.1175/jpo-d-23-0211.1

Contreras, M., Renault, L., & Marchesiello, P. (2023). Understanding energy pathways in the gulf stream. *Journal of Physical Oceanography*, *53*(3), 719–736. https://doi.org/10.1175/jpo-d-22-0146.1

Craig, A., Valcke, S., & Coquart, L. (2017). Development and performance of a new version of the OASIS coupler, OASIS3-MCT_3. 0. *Geoscientific Model Development*, *10*(9), 3297–3308. https://doi.org/10.5194/gmd-10-3297-2017

Debreu, L., Marchesiello, P., Penven, P., & Cambon, G. (2012). Two-way nesting in split-explicit ocean models: Algorithms, implementation and validation. *Ocean Modelling*, *49*, 1–21. https://doi.org/10.1016/j.ocemod.2012.03.003

Desbiolles, F., Meroni, A. N., Renault, L., & Pasquero, C. (2023). Environmental control of wind response to sea surface temperature patterns in reanalysis dataset. *Journal of Climate*, *36*(12), 3881–3893. https://doi.org/10.1175/jcli-d-22-0373.1

Dong, J., Fox-Kemper, B., Wenegrat, J. O., Bodner, A. S., Yu, X., Belcher, S., & Dong, C. (2024). Submesoscales are a significant turbulence source in global ocean surface boundary layer. *Nature Communications*, *15*(1), 9566. https://doi.org/10.1038/s41467-024-53959-y

Farrar, J. T., D'Asaro, E., Rodriguez, E., Shcherbina, A., Lenain, L., Omand, M., et al. (2025). *S-mode: The sub-mesoscale ocean dynamics experiment*. Bulletin of the American Meteorological Society.

Harrison, C. S., Long, M. C., Lovenduski, N. S., & Moore, J. K. (2018). Mesoscale effects on carbon export: A global perspective. *Global Biogeochemical Cycles*, *32*(4), 680–703. https://doi.org/10.1002/2017gb005751

Kessouri, F., Bianchi, D., Renault, L., McWilliams, J. C., Frenzel, H., & Deutsch, C. A. (2020). Submesoscale currents modulate the seasonal cycle of nutrients and productivity in the California current system. *Global Biogeochemical Cycles*, *34*(10), e2020GB006578. https://doi.org/10.1029/2020gb006578

Large, W. G., McWilliams, J. C., & Doney, S. C. (1994). Oceanic vertical mixing: A review and a model with a nonlocal boundary layer parameterization. *Reviews of Geophysics*, *32*(4), 363–403. https://doi.org/10.1029/94rg01872

Larrañaga, M., Renault, L., Wineteer, A., Contreras, M., Arbic, B. K., Bourassa, M. A., & Rodriguez, E. (2025). Assessing the future odysea satellite mission for the estimation of ocean surface currents, wind stress, energy fluxes, and the mechanical coupling between the ocean and the atmosphere. *Remote Sensing*, *17*(2), 302. https://doi.org/10.3390/rs17020302

Lemarié, F., Kurian, J., Shchepetkin, A. F., Molemaker, M. J., Colas, F., & McWilliams, J. C. (2012). Are there inescapable issues prohibiting the use of terrain-following coordinates in climate models? *Ocean Modelling*, *42*, 57–79. https://doi.org/10.1016/j.ocemod.2011.11.007

Lévy, M., Klein, P., & Ben Jelloul, M. (2009). New production stimulated by high-frequency winds in a turbulent mesoscale eddy field. *Geophysical Research Letters*, *36*(16). https://doi.org/10.1029/2009gl039490

López-Dekker, P., Rott, H., Prats-Iraola, P., Chapron, B., Scipal, K., & De Witte, E. (2019). Harmony: An Earth explorer 10 mission candidate to observe land, ice, and ocean surface dynamics. In *IGARSS 2019–2019 IEEE International Geoscience and Remote Sensing Symposium* (pp. 8381–8384).

Ma, X., Jing, Z., Chang, P., Liu, X., Montuoro, R., Small, R. J., et al. (2016). Western boundary currents regulated by interaction between ocean eddies and the atmosphere. *Nature*, *535*(7613), 533–537. https://doi.org/10.1038/nature18640

Mahadevan, A. (2016). The impact of submesoscale physics on primary productivity of plankton. *Annual Review of Marine Science*, *8*(1), 161–184. https://doi.org/10.1146/annurev-marine-010814-015912

Marchesiello, P., Debreu, L., & Couvelard, X. (2009). Spurious diapycnal mixing in terrain-following coordinate models: The problem and a solution. *Ocean Modelling*, *26*(3–4), 156–169. https://doi.org/10.1016/j.ocemod.2008.09.004

Masson, S., Jullien, S., Maisonnave, E., Gill, D., Samson, G., Le Corre, M., & Renault, L. (2025). An updated non-intrusive, multi-scale, and flexible coupling interface in WRF 4.6. 0. *Geoscientific Model Development*, *18*(4), 1241–1263. https://doi.org/10.5194/gmd-18-1241-2025

Nuijens, L., Wenegrat, J. O., Lopez Dekker, P., Pasquero, C., O'Neill, L. W., Ardhuin, F., et al. (2024). *The Air-Sea Interaction (ASI) sub-mesoscale: Physics and impact* (Tech. Rep.). NSF National Center for Atmospheric Research. https://doi.org/10.5065/78AC-QD31

Renault, L., Contreras, M., Marchesiello, P., Conejero, C., Uchoa, I., & Wenegrat, J. (2024). Unraveling the impacts of submesoscale thermal and current feedbacks on the low-level winds and oceanic submesoscale currents. *Journal of Physical Oceanography*, *54*(12), 2463–2486. https://doi.org/10.1175/jpo-d-24-0097.1

Renault, L., Marchesiello, P., Masson, S., & Mcwilliams, J. C. (2019). Remarkable control of western boundary currents by eddy killing, a mechanical air-sea coupling process. *Geophysical Research Letters*, *46*(5), 2743–2751. https://doi.org/10.1029/2018gl081211

Renault, L., Masson, S., Arsouze, T., Madec, G., & McWilliams, J. C. (2020). Recipes for how to force oceanic model dynamics. *Journal of Advances in Modeling Earth Systems*, *12*(2), e2019MS001715. https://doi.org/10.1029/2019ms001715

Renault, L., Masson, S., Oerder, V., Colas, F., & McWilliams, J. (2023). Modulation of the oceanic mesoscale activity by the mesoscale thermal feedback to the atmosphere. *Journal of Physical Oceanography*, *53*(7), 1651–1667. https://doi.org/10.1175/jpo-d-22-0256.1

Renault, L., McWilliams, J. C., & Gula, J. (2018). Dampening of submesoscale currents by air-sea stress coupling in the Californian upwelling system. *Scientific Reports*, *8*(1), 13388. https://doi.org/10.1038/s41598-018-31602-3

Renault, L., McWilliams, J. C., & Masson, S. (2017). Satellite observations of imprint of oceanic current on wind stress by air-sea coupling. *Scientific Reports*, *7*(1), 17747. https://doi.org/10.1038/s41598-017-17939-1

Renault, L., Molemaker, M. J., Gula, J., Masson, S., & McWilliams, J. C. (2016a). Control and stabilization of the gulf stream by oceanic current interaction with the atmosphere. *Journal of Physical Oceanography*, *46*(11), 3439–3453. https://doi.org/10.1175/jpo-d-16-0115.1

Renault, L., Molemaker, M. J., McWilliams, J. C., Shchepetkin, A. F., Lemarié, F., Chelton, D., et al. (2016b). Modulation of wind work by oceanic current interaction with the atmosphere. *Journal of Physical Oceanography*, *46*(6), 1685–1704. https://doi.org/10.1175/jpo-d-15-0232.1

Rodríguez, E., Bourassa, M., Chelton, D., Farrar, J. T., Long, D., Perkovic-Martin, D., & Samelson, R. (2019). The winds and currents mission concept. *Frontiers in Marine Science*, *6*, 438. https://doi.org/10.3389/fmars.2019.00438

Seo, H., O'Neill, L. W., Bourassa, M. A., Czaja, A., Drushka, K., Edson, J. B., et al. (2023). Ocean mesoscale and frontal-scale ocean–atmosphere interactions and influence on large-scale climate: A review. *Journal of Climate*, *36*(7), 1981–2013. https://doi.org/10.1175/jcli-d-21-0982.1

Skamarock, W. C., Klemp, J. B., Dudhia, J., Gill, D. O., Barker, D. M., Duda, M. G., et al. (2008). A description of the advanced research WRF version 3. *NCAR technical note*, *475*, 113.

Small, R. d., de Szoeke, S. P., Xie, S., O'neill, L., Seo, H., Song, Q., et al. (2008). Air–sea interaction over ocean fronts and eddies. *Dynamics of Atmospheres and Oceans*, *45*(3–4), 274–319. https://doi.org/10.1016/j.dynatmoce.2008.01.001

Su, Z., Torres, H., Klein, P., Thompson, A. F., Siegelman, L., Wang, J., et al. (2020). High-frequency submesoscale motions enhance the upward vertical heat transport in the global ocean. *Journal of Geophysical Research: Oceans*, *125*(9), e2020JC016544. https://doi.org/10.1029/2020jc016544

Su, Z., Wang, J., Klein, P., Thompson, A. F., & Menemenlis, D. (2018). Ocean submesoscales as a key component of the global heat budget. *Nature Communications*, *9*(1), 775. https://doi.org/10.1038/s41467-018-02983-w

Uchoa, I., Wenegrat, J. O., & Renault, L. (2025). Sink of eddy energy by submesoscale sea surface temperature variability in a coupled regional model. *Journal of Physical Oceanography*, *55*(8), 993–1007. https://doi.org/10.1175/jpo-d-24-0040.1

Wenegrat, J. O., Thomas, L. N., Sundermeyer, M. A., Taylor, J. R., D'Asaro, E. A., Klymak, J. M., et al. (2020). Enhanced mixing across the gyre boundary at the Gulf stream front. *Proceedings of the National Academy of Sciences*, *117*(30), 17607–17614. https://doi.org/10.1073/pnas.2005558117